Editors' Suggestion

Multipolar magnetism in $5d^2$ vacancy-ordered halide double perovskites

Koushik Pradhan,[1] Arun Paramekanti,[2] and Tanusri Saha-Dasgupta[1,*]

[1]*Department of Condensed Matter Physics and Materials Science, S.N. Bose National Centre for Basic Sciences, Kolkata 700098, India*

[2]*Department of Physics, University of Toronto, 60 St. George Street, Toronto, Ontario, Canada M5S 1A7*

(Received 10 March 2024; revised 21 April 2024; accepted 22 April 2024; published 8 May 2024)

Vacancy-ordered halide double perovskites hosting $4d/5d$ transition metals have emerged as a distinct platform for investigating unconventional magnetism arising out of the interplay of strong atomic spin-orbit coupling (SOC) and Coulomb interactions. Focusing on the d^2 system Cs_2WCl_6, our *ab initio* electronic structure calculation reveals very narrow electronic bands, fulfilling the necessary condition to realize exotic orders. Using this input, we solve the many-body spin-orbit coupled single-site problem by exact diagonalization and show that the multiplet structure of Cs_2WCl_6 hosts ground non-Kramers doublets on W, with vanishing dipole moment and a small gap to an excited magnetic triplet. Our work provides the rationale for the observed strong deviation from the classic Kotani behavior in Cs_2WCl_6 for the measured temperature dependence of the magnetic moment. The non-Kramers doublets on W exhibit nonzero quadrupolar and octupolar moments, and our calculated two-site exchange supports the dominance of intersite octupolar exchange over quadrupolar interactions. We predict ferro-octupolar order with $T_c \sim 5$ K, which may get somewhat suppressed by quantum fluctuations and disorder; this could be tested in future low-temperature experiments.

DOI: 10.1103/PhysRevB.109.184416

I. INTRODUCTION

Compounds crystallizing in the perovskite structure with the general formula ABX_3, where A is an alkali or alkaline metal, B is a transition metal, and X is oxygen, nitrogen, or halogen, are among the materials most intensely studied by condensed matter physicists and solid-state chemists due to their fascinating physical and chemical properties [1–6]. Ordered double perovskites $A_2BB'X_6$ have structures derived from the perovskite structure, formed when exactly half of the B site cations are replaced by another B' cation and a rocksalt ordering between these two is achieved [7]. Oxide-based double perovskites (DPs) with a $3d$ transition metal at the B site and a $4d/5d$ transition metal at the B' site have been studied for the intriguing properties arising out of the interplay of strong correlation and strong spin-orbit coupling (SOC) [8]. To realize unconventional magnetic properties that include exotic spin-orbit coupled ground states, e.g., quantum spin liquids, or to enhance magnetic frustration, it is often desirable to reduce the electronic bandwidth, which thereby amplifies the role of local strong correlations as well as SOC effects. In this context, for instance, $5d^4$ compounds like Ba_2YIrO_6 with Ir^{5+} have been studied [9] by putting a nonmagnetic cation like Y at the B site, which leads to a reduced bandwidth compared with perovskites such as $SrIrO_3$. Nevertheless, the properties of such DPs remain debated; while some studies have argued for a nonmagnetic insulator in Ba_2YIrO_6, with proximity to excitonic magnetism or impurity-induced magnetism [10–12], *ab initio* and dynamical mean-field theory studies instead have found evidence of a considerable bandwidth, which can lead to long-range magnetic order [13] or, at the very least, to fluctuating local moments in the ground state [14]. Experiments on $5d^1$ DPs, such as Ba_2NaOsO_6 with Os^{7+} [15,16] and Ba_2MgReO_6 with Re^{6+} [17–20], have also revealed unusual forms of "multipolar magnetism," which refers to the formation of higher-order multipoles such as quadrupoles and octupoles, thus going beyond conventional dipolar magnetism. This, in turn, reflects the role of atomic SOC and the correlation effect at the single-site level. While multipolar magnetism has also been proposed and actively investigated in certain cubic $5d^2$ osmate DPs [21–27], such as Ba_2MgOsO_6 and Ba_2ZnOsO_6, conclusive evidence of multipolar order in these $5d^2$ oxide DPs is lacking.

In this backdrop, vacancy-ordered DPs in which the second B' site is vacant, resulting in isolated BX_6 octahedra bound electrostatically by A site cations, appear to be an ideal platform to investigate unconventional forms of magnetism. Vacancy-ordered DPs with the K_2PtCl_6 structure type were discovered way back in 1834 [28–30]. In recent times, vacancy-ordered DPs with a monovalent cation at the A site and a halide anion at the X site along with transition metal ions at the B site have been synthesized [31]. These halide DPs can also incorporate organic ligands and are of potential interest as photovoltaics [28]. The creation of a vacant site at B' as well as the introduction of a halogen instead of oxygen leads to the expansion of the lattice parameter by ∼20%–25%. One would then expect these compounds to be as close to the atomic limit as possible for a crystalline system. Transition-metal-based vacancy-ordered DPs may thus be thought of as model narrow-bandwidth systems to study exotic properties arising from strong correlation and atomic SOC. The vacancy-ordered DPs with Os^{4+} or Ir^{4+} ions at the B site tend to support this conjecture [32,33]. In addition to d^4 and d^5

*Corresponding author: t.sahadasgupta@gmail.com

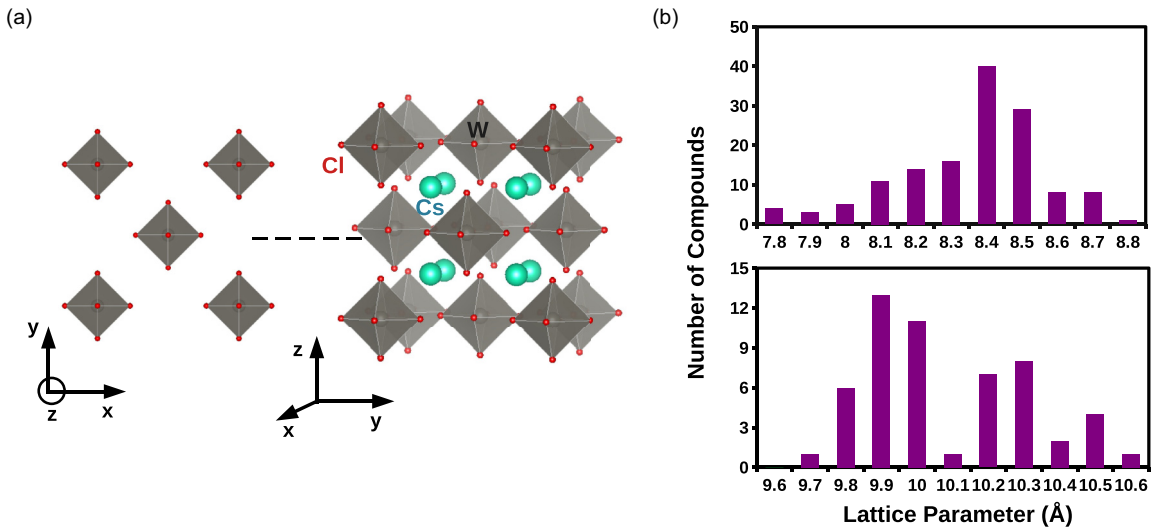

FIG. 1. (a) Structure of Cs_2WCl_6 vacancy-ordered double-perovskite halide in the $Fm\bar{3}m$ (225) cubic space group. (b) Distribution of lattice parameters of double-perovskite oxides (top) and vacancy-ordered double-perovskite chlorides (bottom) showing the significant lattice expansion in the latter class of compounds. For fair comparison only double-perovskite oxides with space group $Fm\bar{3}m$ are included.

compounds based on late transition metals, vacancy-ordered DPs with early transition metals like W, Mo, and Ta have also been reported, which makes compounds with d^1 and d^2 filling also accessible for investigation [34–36]. Compounds with d^2 filling with the possible formation of a $J = 2$ moment are special since they are isomorphic to a d-orbital state with angular momentum $L = 2$.

DPs such as Cs_2WCl_6 which have been synthesized through the solid-state route [37] and hydrothermal synthesis [38] have been reported to show differing colors, suggesting that its properties show strong sample dependence and dependence on the synthesis method. A recent report claimed to have synthesized phase pure Cs_2WCl_6 under anaerobic and anhydrous conditions [39]. Remarkably, the magnetic characterization of this compound revealed peculiar temperature dependence of its magnetic susceptibility, at odds with the well-known Kotani model [40]. In this study, we focus on Cs_2WCl_6, with $5d^2$ filling on W, and show that such vacancy-ordered DPs are ideal candidates to host multipolar magnetism, with the unusual nature of magnetic susceptibility arising from non-Kramers doublets on W. We make predictions for future experiments to verify our conclusions.

II. CRYSTAL STRUCTURE

Vacancy-ordered halide DP Cs_2WCl_6 crystallizes in a fcc crystal structure [39] with space group $Fm\bar{3}m$ (225). Cs and W occupy the high-symmetry 8c and 4a Wyckoff positions with coordinates (0.25, 0.25, 0.25) and (0, 0, 0), while Cl atoms sit at 24e Wyckoff positions with (x, 0, 0) coordinates, with x being a free parameter. Each W atom is surrounded by Cl atoms in perfect octahedra, and Cs atoms reside in the hollow between the [WCl_6] octahedra, with 12-fold coordination of Cl atoms, as shown in Fig. 1(a).

Full geometry optimization, with fixed crystal symmetry, shows the important role of the exchange-correlation functional in density functional theory (DFT). With the choice of the Perdew-Burke-Ernzerhof (PBE) and PBEsol (PBE solid) exchange-correlation functionals, the optimized volume is found to show a deviation of ∼9.5% and ∼1% from the experimentally measured volume, respectively, indicating the superiority of PBEsol over PBE. In subsequent DFT calculations, we thus used the PBEsol exchange-correlation functional. For DFT computational details see the Appendix. The W-Cl bond length in optimized geometry turned out to be 2.377 Å, in comparison to W-O bond length of 1.955 Å in Sr_2CrWO_6. The optimized lattice parameter turned out to be 10.32 Å, which is significantly larger than that of Sr_2CrWO_6 (7.8200 Å) [41]. In this context, it is interesting to note that the generally studied oxide DPs have substantially smaller lattice parameters compared to those of chlorides due to the smaller ionic radius of the O atom. This is evident in Fig. 1(b), where the distribution of the lattice parameters of known oxide DPs and vacancy-ordered chloride DPs, both having space group symmetry $Fm\bar{3}m$, is plotted. While the lattice parameter values for oxides lie in the range 7.8–8.8 Å, the corresponding values for vacancy-ordered chloride DPs lie in the range 9.6–10.6 Å.

III. ELECTRONIC STRUCTURE

For first-principles modeling of the compound, it is appropriate to use non-spin-polarized electronic structure, with magnetism being described at a model level, including spin-orbit coupling and electron correlation. This is expected to capture the multiplet physics and possible formation of a $J = 2$ moment with a vanishing dipole moment.

Figure 2 shows the non-spin-polarized band structure and the corresponding orbital projected density of states in the wide energy range of −0.5 to 4 eV around the Fermi energy E_F. The W d states are crystal field split into triply degenerate t_{2g} (xy, yz, zx) and doubly degenerate e_g ($3z^2$-r^2, x^2-y^2) states in the octahedral crystal field of Cl atoms. With d^2 occupancy

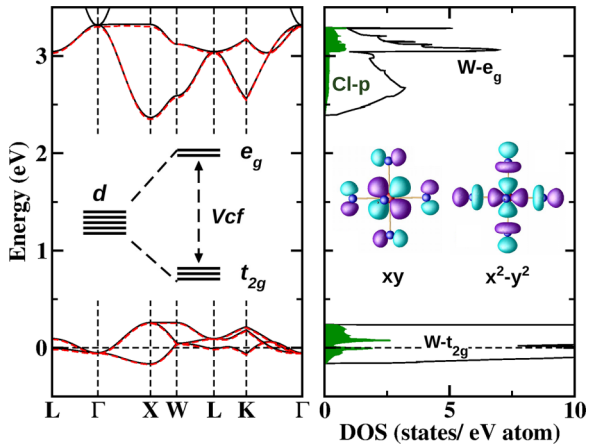

FIG. 2. Left: Non-spin-polarized band structure (solid black lines) together with the tight-binding bands (dashed red lines) plotted along the high-symmetry path of the Brillouin zone. The inset shows the t_{2g}-e_g crystal field splitting. Right: The density of states projected on W d (solid black lines) and Cl p (green shading) states. The inset shows the t_{2g} (x^2-y^2) and e_g (xy) Wannier functions, with lobes with different signs colored differently.

of W^{4+}, the Fermi level is crossed by t_{2g} states admixed with Cl p due to finite W-Cl hybridization. The Cl p-dominated states lie far below E_F, outside the range of the plot. W t_{2g} bands are found to possess a very narrow bandwidth of ∼1 eV, compared with the W bandwidth of ∼2 eV in Sr_2CrWO_6 [42].

Starting from this DFT electronic structure, we obtain the W d-only model through Nth-orbital muffin-tin orbital (NMTO) downfolding [43], in which all degrees of freedom other than W d are downfolded. The real-space representation of this Hamiltonian in the Wannier basis of W d provides information on the on-site matrix and thus the t_{2g}-e_g crystal field splitting and on the W-W hopping integrals. The t_{2g} (xy) and e_g (x^2-y^2) W Wannier functions constructed through NMTO downfolding is shown in the inset of Fig. 2. While the central parts of the Wannier functions are shaped according to the respective symmetries of the W d orbitals, the tails residing in the Cl atoms are shaped like p, showing the formation of W-Cl π and σ bonding for t_{2g} and e_g Wannier functions, respectively.

The t_{2g}-e_g crystal field $V_{\rm cf}$ splitting turned out to be ∼3.0 eV, significantly smaller than that found for corresponding $5d$ transition metal oxides, which is about 5 eV [12], arising from the significantly smaller W-Cl bond length vis-à-vis that in oxides. The resultant smaller value of $V_{\rm cf}$ can further enhance the role of t_{2g}-e_g interactions in determining the low-energy physics, as discussed in Sec IV. The narrow bandwidth of W d suffices for the nearest-neighbor (NN) tight-binding W d-only Hamiltonian to faithfully represent the full DFT electronic structure, as shown in Fig. 2 by superimposing the NN tight-binding bands (red) on the full band structure (black). Table I lists the hopping matrix, obtained with the NMTO downfolding calculation, between two nearest-neighbor W atoms with a connecting vector (0.5, 0.5, 0) in the xy plane. With cubic symmetry, the corresponding matrices in the other planes can be obtained via C_3 transformations about the [111] axis.

TABLE I. Hopping matrix, obtained with the NMTO downfolding calculation, between two nearest-neighbor W atoms with the connecting vector (0.5, 0.5, 0). All the energies are in eV.

Orbital	xy	xz	yz	z^2	x^2-y^2
xy	−0.0458	0.0	0.0	−0.0223	0.0
xz	0.0	0.0109	0.0111	0.0	0.0
yz	0.0	0.0111	0.0109	0.0	0.0
z^2	−0.0233	0.0	0.0	−0.0337	0.0
x^2-y^2	0.0	0.0	0.0	0.0	0.1089

IV. PSEUDOSPIN HAMILTONIAN

Armed with this DFT input, we next solve the many-body spin-orbit entangled W d Hamiltonian in terms of its multiplet structure and pseudospin representation.

A. Single-site model

The local single-site Hamiltonian for the d^2 configuration which incorporates the interplay of crystal electric field (CEF) splitting, atomic SOC, and interactions is given by

$$H_{\rm loc} = H_{\rm CEF} + H_{\rm SOC} + H_{\rm int}, \tag{1}$$

where $H_{\rm CEF}$ is the octahedral t_{2g}-e_g splitting, $H_{\rm SOC}$ captures the atomic SOC, and $H_{\rm int}$ encapsulates electron-electron interactions.

We work in the orbital basis, labeling the t_{2g} orbitals by $\ell \equiv \{1, 2, 3\}$ and e_g orbitals by $\ell = 4, 5$. The octahedral CEF term is then given by

$$H_{\rm CEF} = V_{\rm cf} \sum_{\ell=4,5} \sum_{s} n_{\ell,s}, \tag{2}$$

where $s = \uparrow, \downarrow$ is the spin. $V_{\rm cf}$ captures the on-site difference between e_g and t_{2g} arising due to the larger ligand repulsion of e_g levels compared to t_{2g}.

The SOC term is

$$H_{\rm SOC} = \frac{\lambda}{2} \sum_{\ell,\ell'} \sum_{s,s'} \langle \ell | \, \mathbf{L} \, | \ell' \rangle \cdot \langle s | \, \sigma \, | s' \rangle \, c^\dagger_{\ell s} c_{\ell' s'}, \tag{3}$$

where σ is the vector of Pauli matrices and $\mathbf{L}$ are the d-orbital angular momentum matrices. The Kanamori interaction is given by

$$H_{\rm int} = U \sum_{\ell} n_{\ell\uparrow} n_{\ell\downarrow} + \left(U' - \frac{J_H}{2} \right) \sum_{\ell > \ell'} n_\ell n_{\ell'} - J_H \sum_{\ell \neq \ell'} \mathbf{S}_\ell \cdot \mathbf{S}_{\ell'} + J_H \sum_{\ell \neq \ell'} c^\dagger_{\ell\uparrow} c^\dagger_{\ell\downarrow} c_{\ell'\downarrow} c_{\ell'\uparrow}, \tag{4}$$

where U and U' are the intraorbital and interorbital Hubbard interactions, respectively, and J_H is Hund's coupling. $\mathbf{S}_\ell = (1/2) c^\dagger_{\ell s} \sigma_{s,s'} c_{\ell' s'}$ denotes the spin operator for orbital ℓ, while the number operator $n_\ell \equiv n_{\ell\uparrow} + n_{\ell\downarrow}$ counts the total number of electrons in orbital ℓ. Assuming spherical symmetry of the Coulomb interaction, $U' = U - 2J_H$ [44].

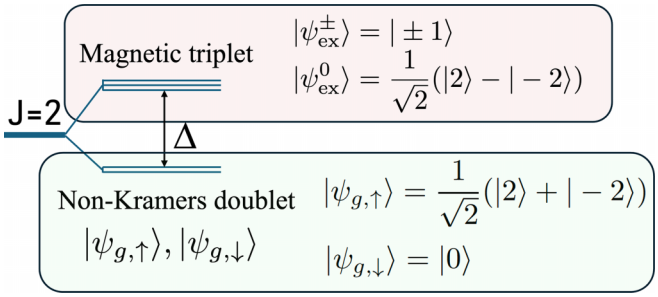

FIG. 3. Schematic diagram of the $J = 2$ multiplet weakly split into a non-Kramers doublet and gapped magnetic triplet. The weak splitting Δ is induced by t_{2g}-e_g interactions which can be captured by a Stevens operator (see text).

Diagonalizing $H_{\rm loc}$, we find a low-energy manifold with five states. These five low-energy states form part of a $J = 2$ total angular momentum manifold, which is weakly split in the octahedral environment: a ground state non-Kramers doublet and an excited triplet which is split from the doublet by a small energy gap $\Delta \sim \lambda^2 J_H/V_{\rm cf}$ [23]. This is schematically depicted in Fig. 3. The next set of excited levels, $J = 0$ and $J = 1$, is split by a large energy gap $\sim\lambda$; we ignore these high-energy states for discussing the spin susceptibility and entropy at moderate temperatures. In the limit of t_{2g}-e_g crystal field splitting $V_{\rm cf} \to \infty$, the gap $\Delta \to 0$, and the two-electron ground state of $H_{\rm loc}$ is a fivefold-degenerate $J = 2$ multiplet obtained from spin-orbit coupling of $L_{\rm eff} = 1$ and $S_{\rm eff} = 1$ of two electrons in the t_{2g} orbital.

We fix the parameters $\lambda = 0.35$ eV, $U = 2.5$ eV, and $J_H = 0.25$ eV. It is worth mentioning at this point that, while the general picture of a $J = 2$ ground state multiplet that splits into a low-energy non-Kramers doublet and an excited triplet is a robust qualitative result independent of the precise choice λ and J_H, the quantitative value of the triplet-doublet splitting does depend on λ and J_H. In the absence of precise and accurate estimates, we use the values obtained from the fit of experimental data like resonant inelastic x-ray scattering (RIXS). At this point, we have not found RIXS data for Cs_2WCl_6 since this is a relatively newly synthesized compound. We have thus referred to the closely related vacancy-ordered halide double perovskite K_2OsCl_6. Our choice of λ and J_H reproduces the peaks seen in RIXS measurements on K_2OsCl_6 up to a scale $\sim$1.2 eV [45]. λ and J_H, being atomic properties, are expected to be similar between two 5*d* transition-metal-based compounds. Our expectation is further supported by the fact that λ and J_H in K_2OsCl_6 are found to be similar to those of oxide double perovskites based on 5*d* transition metals [12,46]. Using our *ab initio* estimate of $V_{\rm cf} \approx 3.0$ eV, a single-site exact diagonalization yields $\Delta \approx 7$ meV. However, the single-site model, as used in the present study, is an *effective* model only for the low-energy physics of the WCl_6 octahedra with seven sites. Thus, the DFT-estimated $V_{\rm cf}$ can get renormalized in the context of the single-site model [45], and it may be considered a tuning parameter. Decreasing $V_{\rm cf} = 1.7$ eV, for example, increases the low-energy doublet-triplet splitting of the $J = 2$ multiplet to $\Delta \approx 15$ meV while leaving the rest of the spectrum up to $\sim$1.2 eV nearly unchanged. Indeed, the correct thing to do at low energy is to write an effective Hamiltonian for the $J = 2$ multiplet in terms of Stevens operators [47], with

$$H_{\rm S} = -\frac{\Delta}{120}(O_{40} + 5O_{44}), \tag{5}$$

$$O_{40} = 35J_z^4 - [30J(J+1) - 25]J_z^2 + 3J^2(J+1)^2 - 6J(J+1), \tag{6}$$

$$O_{44} = \tfrac{1}{2}(J_+^4 + J_-^4), \tag{7}$$

which splits the $J = 2$ multiplet, leading to the doublet-triplet gap Δ [23,25]. In this spirit, in the following, we will use Δ as a fitting parameter to explore the consequences for the spin susceptibility and entropy. We would further like to add that the overestimation of $V_{\rm cf}$ by DFT is a well-known feature which arises due to the neglect of *d*-*p* Coulomb interaction between the transition metal and the ligand, affecting the *d*-*p* charge transfer energy and thus influencing $V_{\rm cf}$ in the metal-only model. This issue has been studied using dynamical mean-field theory in the context of high-T_c cuprates [48].

In terms of J_z eigenstates, the wave functions of the pseudospin-1/2 non-Kramers doublet ground state are given by (see Fig. 3) [49]

$$|\psi_{g,\uparrow}\rangle = \frac{1}{\sqrt{2}}(|2\rangle + |-2\rangle), \quad |\psi_{g,\downarrow}\rangle = |0\rangle, \tag{8}$$

while the excited state triplet wave functions are given by

$$|\psi_{e,\pm1}\rangle = |\pm 1\rangle, \quad |\psi_{e,0}\rangle = \frac{1}{\sqrt{2}}(|2\rangle - |-2\rangle). \tag{9}$$

B. Spin susceptibility and effective moment: Breakdown of the Kotani result

Using these wave functions and the energy gap Δ, the spin susceptibility can be computed as

$$\chi(T) = (g\mu_B)^2 \left[\frac{\frac{8}{\Delta} + \left(\frac{2}{T} - \frac{8}{\Delta}\right)e^{-\Delta/T}}{2 + 3e^{-\Delta/T}}\right]. \tag{10}$$

We define $\mu^2_{\rm eff}(T) = \frac{1}{g^2}\chi(T)T$, which leads to

$$\mu^2_{\rm eff}(T) = \mu_B^2 T \left[\frac{\frac{8}{\Delta} + \left(\frac{2}{T} - \frac{8}{\Delta}\right)e^{-\Delta/T}}{2 + 3e^{-\Delta/T}}\right]. \tag{11}$$

To make a comparison with the published experimental data [39], we plot this in units of μ_B^2, setting $y_{\rm eff} = \mu_{\rm eff}/\mu_B$, so that

$$y^2_{\rm eff}(T) = T \left[\frac{\frac{8}{\Delta} + \left(\frac{2}{T} - \frac{8}{\Delta}\right)e^{-\Delta/T}}{2 + 3e^{-\Delta/T}}\right]. \tag{12}$$

We note that our result in Eq. (12) is valid for only $T/\lambda \ll 1$ since we do not account for higher spin-orbit levels which are split off by scales comparable to λ. These high-energy states will give rise to a background Van Vleck contribution [40,50]. We can account for such a constant background susceptibility via a phenomenological additional constant α, which leads to

$$y^2_{\rm eff}(T) = T \left[\frac{\frac{8}{\Delta} + \left(\frac{2}{T} - \frac{8}{\Delta}\right)e^{-\Delta/T}}{2 + 3e^{-\Delta/T}}\right] + \alpha T. \tag{13}$$

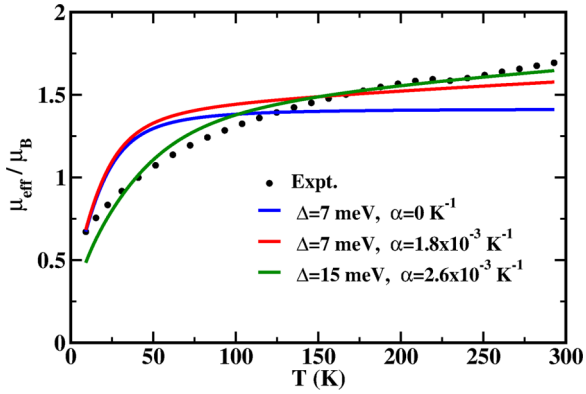

FIG. 4. Comparison of experimental and calculated temperature dependence of the effective magnetic moment $\mu_{\rm eff}$ in units of μ_B for Cs_2WCl_6. The black solid circles represent experimental data, while the blue, red, and green curves are obtained using Eq. (13) for different values of Δ and α as indicated.

We will use this functional form to fit the experimental data, assuming that single-site physics dominates, with Δ and α being treated as fit parameters. We ignore residual impurity effects arising from traces of O in place of Cl [39] which might lead to an additional Curie contribution to $\chi(T)$ at the lowest temperatures.

Figure 4 shows the effective magnetic moment (in units of μ_B) corresponding to various values of Δ and α, plotted as a function of temperature, in comparison to the experimental data [39]. In all cases, we find that the low-temperature moment drops to zero, consistent with the experimental trend and at odds with the Kotani result [39,40]. To choose Δ and α, we first used $\Delta = 7\,\text{meV}$, obtained on the basis of our *ab initio* estimate of $V_{\rm cf}$ with $\alpha = 0$, which ignores all higher-energy levels split off by a scale $\sim\lambda$ as well as the possible contribution of impurities. To explain the linear slope at higher temperatures, we find it is important to include the Van Vleck contribution, given by a nonzero value of α. We show the case with $\Delta = 7\,\text{meV}$ and $\alpha = 1.8 \times 10^{-3}\,\text{K}^{-1}$ as an example, where Δ is still constrained. The best fit to experimental data is obtained using $\Delta = 15\,\text{meV}$ and $\alpha = 2.6 \times 10^{-3}\,\text{K}^{-1}$. The computed data capture the measured temperature variation over almost the entire temperature range. We note that, up to some factors, the scale of α is $O(1/\lambda)$.

C. Single-site entropy

In the low-energy limit, the single-site entropy from the non-Kramers and gapped triplet is given by

$$\frac{S}{k_B} = \frac{3(\Delta/T)}{3+2e^{\Delta/T}} + \ln(2+3e^{-\Delta/T}). \tag{14}$$

This exhibits a plateau at $S = k_B \ln 2$ for $T \lesssim \Delta/4$. To estimate values for Cs_2WCl_6, if we set $\Delta \approx 15\,\text{meV}$, which fits the effective moment data reasonably well, as shown above, this entropy plateau should occur for $T \lesssim 40\,\text{K}$. This entropy will get quenched at low temperature once the non-Kramers doublets develop intersite correlations and form a long-range ordered state. We next estimate these intersite interactions between the non-Kramers doublets.

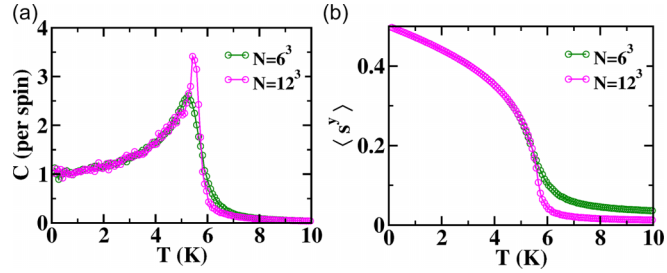

FIG. 5. Classical Monte Carlo simulation results for (a) the specific heat per spin C as a function of temperature showing a phase transition at $T_c \approx 5.5\,\text{K}$ and (b) the ferro-octupolar order parameter $\langle s^y \rangle$ as a function of temperature, showing its onset for $T < T_c$. Simulations are for the model Hamiltonian $H_{\rm spin}$ with parameters given in the text, and system sizes $N = 6^3, 12^3$ spins.

D. Pseudospin interactions and multipolar order

We define the pseudospin-1/2 operators which act on the non-Kramers doublet in terms of the $J = 2$ angular momentum operators as

$$s^x \equiv \left(J_x^2 - J_y^2\right)/4\sqrt{3}, \tag{15}$$

$$s^y \equiv \overline{J_x J_y J_z}/2\sqrt{3}, \tag{16}$$

$$s^z \equiv \left[3J_z^2 - J(J+1)\right]/12, \tag{17}$$

with the overline denoting symmetrization. On symmetry grounds, the most general pseudospin-1/2 exchange Hamiltonian for nearest neighbors is given by

$$\begin{aligned} H_{\rm spin} = \sum_{\langle i,j \rangle} \big[& K_y s_i^y s_j^y + (K_x \cos^2\phi_{ij} + K_z \sin^2\phi_{ij}) s_i^x s_j^x \\ & + (K_x - K_z) \sin\phi_{ij} \cos\phi_{ij} \left(s_i^x s_j^z + s_i^z s_j^x\right) \\ & + (K_x \sin^2\phi_{ij} + K_z \cos^2\phi_{ij}) s_i^z s_j^z \big], \end{aligned} \tag{18}$$

where $\phi_{ij} = \{0, 2\pi/3, 4\pi/3\}$ correspond to nearest neighbors (i,j) in the $\{xy, yz, zx\}$ planes. Here, K_x and K_z are quadrupolar couplings, K_y is the octupolar coupling, and the spin operators (s^x, s^y, s^z) act within the non-Kramers doublet space [24,25,27,51]. Using the single-site Hamiltonian and hopping matrices from our *ab initio* calculations, with Hubbard $U = 2.5\,\text{eV}$ in the Kanamori interaction, we employ an exact Schrieffer-Wolff method to extract the two-site exchange couplings [24]; we find $(K_x, K_y, K_z) \approx (-0.04, -0.56, 0.24)\,\text{meV}$. We note that the largest exchange interactions are of order 0.5 meV, which is $\ll \Delta$. The dominant ferro-octupolar exchange K_y suggests that the ground state of Cs_2WCl_6 should have ferro-octupolar order.

Figure 5 shows results from the classical Monte Carlo simulations of $H_{\rm spin}$, treating the pseudospin-1/2 operators as classical vectors (of length $=1/2$) with anisotropic and bond-dependent interactions; we used 4×10^4 sweeps for equilibration and measurements on system sizes with $N = 6^3$ and $N = 12^3$ spins. The specific heat peak in Fig. 5(a) signals a phase transition at $T_c \approx 5.5$ K, and from Fig. 5(b) we find the development of ferro-octupolar order for $T < T_c$. In experiments, T_c may be somewhat suppressed by the effects of quantum fluctuations and possible weak disorder.

V. SUMMARY AND DISCUSSION

Vacancy-ordered halide DPs having $4d$ or $5d$ transition metals at the B site are a unique class of compounds in which a small bandwidth and strong SOC can lead to interesting physics. Understanding the local physics of this class of materials is the first step in exploring the wide range of phenomena which might be realized in future experiments. Taking this first step, we showed that the d^2 DPs in this category can realize multipolar magnetism. In particular, the low-energy physics of these materials may be described in terms of a non-Kramers doublet split off from a gapped magnetic triplet. At the single-site level, this explains the puzzling strong deviation from the Kotani plot, as found in a recent experiment [39]. We found that there are weak interactions between the non-Kramers doublets which stem from the very flat bands and weak intersite hopping found in our *ab initio* calculations. Such intersite interactions, which we computed, are expected to lead to long-range ferro-octupolar order with $T_c \approx 5.5$ K. The existence of non-Kramers doublets and their consequences for magnetism were previously proposed and partially explored in $5d^2$ osmate DPs such as Ba_2MgOsO_6 and Ba_2ZnOsO_6, but there is no conclusive evidence for this yet [21–25,27]. Our findings for Cs_2WCl_6 thus take an important step forward by expanding the set of candidate $5d$ quantum materials which may exhibit unconventional multipolar magnetism.

Recently, we came across a preprint by Li *et al.* [52] which explores these halide DP compounds using a combination of DFT, exact diagonalization, and cluster diagonalization. At the single-site level, their theory for Cs_2WCl_6 leads to results which are largely in agreement with the Kotani plot and at odds with our results. We attribute this to the fact that the original work by Kotani [40] and the work by Li *et al.* [52] consider a t_{2g}-only model, completely ignoring the effect of e_g orbitals, while we show that taking into account the effect of the e_g orbitals either via microscopics or via effective Stevens operators is important in splitting the fivefold $J = 2$ multiplet and thereby stabilizing a non-Kramers doublet as a ground state. It should be noted that due to the substantially larger metal-ligand bond length in vacancy-ordered halides in comparison to oxides, the crystal field splitting is generally smaller than that in commonly considered oxides, which might be further renormalized to smaller values within an effective single-site metal-only model. Such renormalization of high-energy parameters in single-site models versus a full octahedral cluster was also noted for modeling RIXS in K_2OsCl_6 [45].

The implications of this difference are quite important. For instance, the paper by Li *et al.* [52] found effective moments $\mu_{\text{eff}}(T)$ which are in agreement with experiments only when they studied a two-site model. However, such a two-site cluster kills the magnetic moment by forming a nearest-neighbor singlet. It is unclear whether this picture of valence bond singlet formation is the appropriate description of magnetism on the full lattice. In our work, by contrast, the effective moment vanishes due to the formation of a single-site non-Kramers doublet which has no magnetic dipole moment degrees of freedom. Furthermore, our computed exchange interactions show that this material might host ferro-octupolar order on the fcc lattice rather than the Li *et al.* [52] proposed scenario of singlets formed from $J = 2$ moments on neighboring sites.

Turning to concrete proposals which can serve to experimentally distinguish our proposal from the proposal of Li *et al.* [52], we suggest specific heat and inelastic neutron scattering measurements. The proposed ferro-octupolar transition temperature is $T_c \approx 5.5$ K, which, however, may be somewhat suppressed by disorder and quantum fluctuations. In light of this, low-temperature measurements like specific heat and muon spin resonance measurements [23,53–57] may be able to explore this hidden phase, although further probes would be needed to distinguish such a transition from ordinary magnetic order. Inelastic neutron scattering measurements [21] could be used to detect a spin gap $\sim\Delta$ in the intermediate-temperature regime $T_c \ll T \ll \Delta$, which would bolster the case for our scenario and also serve to extract Δ. We expect that the magnetic entropy per spin will show a plateau $S \sim k_B \ln 2$ at intermediate temperatures in the window $T_c \ll T \lesssim \Delta/4$, where the uncorrelated non-Kramers doublet physics is expected to survive. Finally, ^{35}Cl, ^{37}Cl, and ^{133}Cs NMR measurements could potentially be used to look for more detailed local signatures of magnetism at low temperatures, as was done using ^{23}Na in certain oxide-based DPs [15,16,26,27].

ACKNOWLEDGMENTS

T.S.-D. acknowledges discussions with T. Cheetham and P. Vishnoi. This research was funded by DST India (K.P. and T.S.-D.) and NSERC of Canada (A.P.). We acknowledge funding from SERB-India Vajra Fellowship No. VJR/2019/000076 (A.P., T.S.-D.), which enabled this collaboration. T.S.-D. acknowledges a J.C. Bose National Fellowship (Grant No. JCB/2020/000004) for support.

APPENDIX: COMPUTATIONAL DETAILS

The first-principles DFT calculations were performed using the projector augmented-wave [58] pseudopotential method in the plane wave basis, as implemented within the Vienna Ab-initio Simulation Package (VASP) [59]. We considered the exchange-correlation functionals within the generalized gradient approximation (GGA) of PBE [60] and PBEsol [61]. A plane wave energy cutoff of 600 eV and Brillouin zone sampling with $8 \times 8 \times 8$ Monkhorst-Pack grids were found to be sufficient for the convergence of energies and forces. For structural relaxations, ions were allowed to move until atomic forces became less than $0.0001\ \text{eV}/\text{A}^0$.

For the extraction of a few-band tight-binding Hamiltonian out of a full GGA calculation which can be used as the input to the many-body Hamiltonian, Nth-orbital muffin-tin orbital (NMTO) downfolding calculations were carried out [43]. The consistency of results obtained in the plane wave and linear muffin-tin orbital (LMTO) bases was cross-checked in terms of the density of states and band structures. Starting from a full DFT calculation, the method arrives at a few-orbital Hamiltonian in an energy-selected, effective Wannier function basis by integrating out the degrees of freedom that are not of

interest. The NMTO technique, which is not yet available in its self-consistent form, relies on the self-consistent potential parameters obtained out from LMTO calculations [62]. The obtained tight-binding parameters were found to be in good agreement with maximally localized Wannier function calculations [63].

[1] M. B. Salamon and M. Jaime, The physics of manganites: Structure and transport, Rev. Mod. Phys. **73**, 583 (2001).

[2] J. M. D. Coey, M. Viret, and S. von Molnár, Mixed-valence manganites, Adv. Phys. **48**, 167 (1999).

[3] A. K. Jena, A. Kulkarni, and T. Miyasaka, Halide perovskite photovoltaics: Background, status, and future prospects, Chem. Rev. **119**, 3036 (2019).

[4] W.-J. Yin, J.-H. Yang, J. Kang, Y. Yan, and S.-H. Wei, Halide perovskite materials for solar cells: A theoretical review, J. Mater. Chem. A **3**, 8926 (2015).

[5] M. A. Pena and J. L. G. Fierro, Chemical structures and performance of perovskite oxides, Chem. Rev. **101**, 1981 (2001).

[6] C. N. R. Rao, A. K. Cheetham, and R. Mahesh, Giant magnetoresistance and related properties of rare-earth manganates and other oxide systems, Chem. Mater. **8**, 2421 (1996).

[7] S. Vasala and M. Karppinen, $A_2B'B''O_6$ perovskites: A review, Prog. Solid State Chem. **43**, 1 (2015).

[8] T. Saha-Dasgupta, Double perovskites with 3d and 4d/5d transition metals: Compounds with promises, Mater. Res. Express **7**, 014003 (2020).

[9] T. Dey, A. Maljuk, D. V. Efremov, O. Kataeva, S. Gass, C. G. F. Blum, F. Steckel, D. Gruner, T. Ritschel, A. U. B. Wolter, J. Geck, C. Hess, K. Koepernik, J. van den Brink, S. Wurmehl, and B. Büchner, Ba_2YIrO_6: A cubic double perovskite material with Ir^{5+} ions, Phys. Rev. B **93**, 014434 (2016).

[10] G. Khaliullin, Excitonic magnetism in Van Vleck–type d^4 Mott insulators, Phys. Rev. Lett. **111**, 197201 (2013).

[11] O. N. Meetei, W. S. Cole, M. Randeria, and N. Trivedi, Novel magnetic state in d^4 Mott insulators, Phys. Rev. B **91**, 054412 (2015).

[12] A. Paramekanti, D. J. Singh, B. Yuan, D. Casa, A. Said, Y.-J. Kim, and A. D. Christianson, Spin-orbit coupled systems in the atomic limit: Rhenates, osmates, iridates, Phys. Rev. B **97**, 235119 (2018).

[13] S. Bhowal, S. Baidya, I. Dasgupta, and T. Saha-Dasgupta, Breakdown of $j = 0$ nonmagnetic state in d^4 iridate double perovskites: A first-principles study, Phys. Rev. B **92**, 121113(R) (2015).

[14] H. Schnait, D. Bauernfeind, T. Saha-Dasgupta, and M. Aichhorn, Small moments without long-range magnetic ordering in the zero-temperature ground state of the double perovskite iridate Ba_2YIrO_6, Phys. Rev. B **106**, 035132 (2022).

[15] L. Lu, M. Song, W. Liu, A. P. Reyes, P. Kuhns, H. O. Lee, I. R. Fisher, and V. F. Mitrović, Magnetism and local symmetry breaking in a Mott insulator with strong spin orbit interactions, Nat. Commun. **8**, 14407 (2017).

[16] W. Liu, R. Cong, E. Garcia, A. Reyes, H. Lee, I. Fisher, and V. Mitrović, Phase diagram of Ba_2NaOsO_6, a Mott insulator with strong spin orbit interactions, Phys. B (Amsterdam, Neth.) **536**, 863 (2018).

[17] D. Hirai and Z. Hiroi, Successive symmetry breaking in a $j_{eff} = 3/2$ quartet in the spin-orbit coupled insulator Ba_2MgReO_6, J. Phys. Soc. Jpn. **88**, 064712 (2019).

[18] D. Hirai, H. Sagayama, S. Gao, H. Ohsumi, G. Chen, T. H. Arima, and Z. Hiroi, Detection of multipolar orders in the spin-orbit-coupled $5d$ Mott insulator Ba_2MgReO_6, Phys. Rev. Res. **2**, 022063(R) (2020).

[19] J.-R. Soh, M. E. Merkel, L. Pourovskii, I. Zivkovic, O. Malanyuk, J. Pasztorova, S. Francoual, D. Hirai, A. Urru, D. Tolj, D. Fiore-Mosca, O. Yazyev, N. A. Spaldin, C. Ederer, and H. M. Ronnow, Spectroscopic signatures and origin of a hidden order in Ba_2MgReO_6, arXiv:2312.01767.

[20] D. F. Mosca, C. Franchini, and L. V. Pourovskii, Interplay of superexchange and vibronic effects in the hidden order of Ba_2MgReO_6 unravelled from first principles, arXiv:2402.15564.

[21] D. D. Maharaj, G. Sala, M. B. Stone, E. Kermarrec, C. Ritter, F. Fauth, C. A. Marjerrison, J. E. Greedan, A. Paramekanti, and B. D. Gaulin, Octupolar versus Néel order in cubic $5d^2$ double perovskites, Phys. Rev. Lett. **124**, 087206 (2020).

[22] A. Paramekanti, D. D. Maharaj, and B. D. Gaulin, Octupolar order in d-orbital Mott insulators, Phys. Rev. B **101**, 054439 (2020).

[23] S. Voleti, D. D. Maharaj, B. D. Gaulin, G. Luke, and A. Paramekanti, Multipolar magnetism in d-orbital systems: Crystal field levels, octupolar order, and orbital loop currents, Phys. Rev. B **101**, 155118 (2020).

[24] S. Voleti, A. Haldar, and A. Paramekanti, Octupolar order and Ising quantum criticality tuned by strain and dimensionality: Application to d-orbital Mott insulators, Phys. Rev. B **104**, 174431 (2021).

[25] G. Khaliullin, D. Churchill, P. P. Stavropoulos, and H.-Y. Kee, Exchange interactions, Jahn-Teller coupling, and multipole orders in pseudospin one-half $5d^2$ Mott insulators, Phys. Rev. Res. **3**, 033163 (2021).

[26] R. Cong, E. Garcia, P. C. Forino, A. Tassetti, G. Allodi, A. P. Reyes, P. M. Tran, P. M. Woodward, C. Franchini, S. Sanna, and V. F. Mitrović, Effects of charge doping on Mott insulator with strong spin-orbit coupling, $Ba_2Na_{1-x}Ca_xOsO_6$, Phys. Rev. Mater. **7**, 084409 (2023).

[27] S. Voleti, K. Pradhan, S. Bhattacharjee, T. Saha-Dasgupta, and A. Paramekanti, Probing octupolar hidden order via Janus impurities, npj Quantum Mater. **8**, 42 (2023).

[28] A. E. Fedorovskiy, N. A. Drigo, and M. K. Nazeeruddin, The role of Goldschmidt's tolerance factor in the formation of A_2BX_6 double halide perovskites and its optimal range, Small Methods **4**, 1900426 (2020).

[29] B. Lee, C. C. Stoumpos, N. Zhou, F. Hao, C. Malliakas, C.-Y. Yeh, T. J. Marks, M. G. Kanatzidis, and R. P. H. Chang, Air-stable molecular semiconducting iodosalts for solar cell applications: Cs_2SnI_6 as a hole conductor, J. Am. Chem. Soc. **136**, 15379 (2014).

[30] A. E. Maughan, A. M. Ganose, D. O. Scanlon, and J. R. Neilson, Perspectives and design principles of vacancy-ordered double perovskite halide semiconductors, Chem. Mater. **31**, 1184 (2019).

[31] W. Rahim, A. Cheng, C. Lyu, T. Shi, Z. Wang, D. O. Scanlon, and R. G. Palgrave, Geometric analysis and formability of the cubic A_2BX_6 vacancy-ordered double perovskite structure, Chem. Mater. **32**, 9573 (2020).

[32] M. Saura-Múzquiz, M. Avdeev, H. E. A. Brand, and B. J. Kennedy, Structural and magnetic properties of some vacancy-ordered osmium halide perovskites, Inorg. Chem. **61**, 15961 (2022).

[33] S.-S. Bao, D. Wang, X.-D. Huang, M. Etter, Z.-S. Cai, X. Wan, R. E. Dinnebier, and L.-M. Zheng, $Na_2Ir^{IV}Cl_6$: Spin–orbital-induced semiconductor showing hydration-dependent structural and magnetic variations, Inorg. Chem. **57**, 13252 (2018).

[34] H. Ishikawa, T. Yajima, A. Matsuo, and K. Kindo, Ligand dependent magnetism of the $J_{\rm eff} = 3/2$ Mott insulator Cs_2MX_6 ($M =$ Ta, Nb, $X =$ Br, Cl), J. Phys.: Condens. Matter **33**, 125802 (2021).

[35] H. Ishikawa, T. Takayama, R. K. Kremer, J. Nuss, R. Dinnebier, K. Kitagawa, K. Ishii, and H. Takagi, Ordering of hidden multipoles in spin-orbit entangled $5d^1$ Ta chlorides, Phys. Rev. B **100**, 045142 (2019).

[36] A. Mansouri Tehrani, J.-R. Soh, J. Pásztorová, M. E. Merkel, I. Živković, H. M. Ronnow, and N. A. Spaldin, Charge multipole correlations and order in Cs_2TaCl_6, Phys. Rev. Res. **5**, L012010 (2023).

[37] C. D. Kennedy and R. D. Peacock, 629. Complex chlorides and bromides of quadrivalent tungsten, J. Chem. Soc. 3392 (1963).

[38] Z. Liu, X. Qin, Q. Chen, Q. Chen, Y. Jing, Z. Zhou, Y. S. Zhao, J. Chen, and X. Liu, Highly stable lead-free perovskite single crystals with NIR emission beyond 1100 nm, Adv. Opt. Mater. **10**, 2201254 (2022).

[39] E. E. Morgan, G. T. Kent, A. Zohar, A. O'Dea, G. Wu, A. K. Cheetham, and R. Seshadri, Hybrid and inorganic vacancy-ordered double perovskites A_2WCl_6, Chem. Mater. **35**, 7032 (2023).

[40] M. Kotani, On the magnetic moment of complex ions. (I), J. Phys. Soc. Jpn. **4**, 293 (1949).

[41] J. B. Philipp, P. Majewski, L. Alff, A. Erb, R. Gross, T. Graf, M. S. Brandt, J. Simon, T. Walther, W. Mader, D. Topwal, and D. D. Sarma, Structural and doping effects in the half-metallic double perovskite A_2CrWO_6($A =$ Sr, Ba, and Ca), Phys. Rev. B **68**, 144431 (2003).

[42] H. Das, M. De Raychaudhury, and T. Saha-Dasgupta, Moderate to large magneto-optical signals in high T_c double perovskites, Appl. Phys. Lett. **92**, 201912 (2008).

[43] O. K. Andersen and T. Saha-Dasgupta, Muffin-tin orbitals of arbitrary order, Phys. Rev. B **62**, R16219 (2000).

[44] A. Georges, L. de' Medici, and J. Mravlje, Strong correlations from Hund's coupling, Annu. Rev. Condens. Matter Phys. **4**, 137 (2013).

[45] P. Warzanowski, M. Magnaterra, P. Stein, G. Schlicht, Q. Faure, C. J. Sahle, T. Lorenz, P. Becker, L. Bohatý, M. Moretti Sala, G. Monaco, P. H. M. van Loosdrecht, and M. Grüninger, Electronic excitations in $5d^4 J = 0$ Os^{4+} halides studied by resonant inelastic x-ray scattering and optical spectroscopy, Phys. Rev. B **108**, 125120 (2023).

[46] B. Yuan, J. P. Clancy, A. M. Cook, C. M. Thompson, J. Greedan, G. Cao, B. C. Jeon, T. W. Noh, M. H. Upton, D. Casa, T. Gog, A. Paramekanti, and Y.-J. Kim, Determination of Hund's coupling in $5d$ oxides using resonant inelastic x-ray scattering, Phys. Rev. B **95**, 235114 (2017).

[47] K. W. H. Stevens, Matrix elements and operator equivalents connected with the magnetic properties of rare earth ions, Proc. Phys. Soc., Sect. A **65**, 209 (1952).

[48] P. Hansmann, N. Parragh, A. Toschi, G. Sangiovanni, and K. Held, Importance of d-p Coulomb interaction for high T_c cuprates and other oxides, New J. Phys. **16**, 033009 (2014).

[49] It should be noted that these are not the original single-particle orbital eigenstates. The virtual excitations into the high-energy e_g orbitals split the fivefold degeneracy of the $J = 2$ moment as $2(E_g) \oplus 3(T_{2g})$, resulting in a ground state non-Kramers E_g doublet carrying quadrupolar and octupolar moments, as was explicitly shown in [23].

[50] J. H. Van Vleck, On dielectric constants and magnetic susceptibilities in the new quantum mechanics part III—Application to dia- and paramagnetism, Phys. Rev. **31**, 587 (1928).

[51] D. Churchill and H.-Y. Kee, Competing multipolar orders in a face-centered cubic lattice: Application to the osmium double perovskites, Phys. Rev. B **105**, 014438 (2022).

[52] Y. Li, R. Seshadri, S. D. Wilson, A. K. Cheetham, and R. Valenti, Origins of temperature-dependent magnetism in open-shell $4d$ and $5d$ halide perovskites, arXiv:2402.14064.

[53] C. M. Thompson, C. A. Marjerrison, A. Z. Sharma, C. R. Wiebe, D. D. Maharaj, G. Sala, R. Flacau, A. M. Hallas, Y. Cai, B. D. Gaulin, G. M. Luke, and J. E. Greedan, Frustrated magnetism in the double perovskite La_2LiOsO_6: A comparison with La_2LiRuO_6, Phys. Rev. B **93**, 014431 (2016).

[54] K. M. Kojima, Y. Fudamoto, M. Larkin, G. M. Luke, J. Merrin, B. Nachumi, Y. J. Uemura, M. Hase, Y. Sasago, K. Uchinokura, Y. Ajiro, A. Revcolevschi, and J.-P. Renard, Antiferromagnetic order with spatially inhomogeneous ordered moment size of Zn- and Si-doped $CuGeO_3$, Phys. Rev. Lett. **79**, 503 (1997).

[55] C. A. Marjerrison, C. M. Thompson, A. Z. Sharma, A. M. Hallas, M. N. Wilson, T. J. S. Munsie, R. Flacau, C. R. Wiebe, B. D. Gaulin, G. M. Luke, and J. E. Greedan, Magnetic ground states in the three $Os^{6+}(5d^2)$ double perovskites Ba_2MOsO_6($M =$ Mg, Zn, and Cd) from Néel order to its suppression, Phys. Rev. B **94**, 134429 (2016).

[56] C. M. Thompson, J. P. Carlo, R. Flacau, T. Aharen, I. A. Leahy, J. R. Pollichemi, T. J. S. Munsie, T. Medina, G. M. Luke, J. Munevar, S. Cheung, T. Goko, Y. J. Uemura, and J. E. Greedan, Long-range magnetic order in the $5d^2$ double perovskite Ba_2CaOsO_6: Comparison with spin-disordered Ba_2YReO_6, J. Phys.: Condens. Matter **26**, 306003 (2014).

[57] T. Aharen, J. E. Greedan, C. A. Bridges, A. A. Aczel, J. Rodriguez, G. MacDougall, G. M. Luke, V. K. Michaelis, S. Kroeker, C. R. Wiebe, H. Zhou, and L. M. D. Cranswick, Structure and magnetic properties of the $S = 1$ geometrically frustrated double perovskites La_2LiReO_6 and Ba_2YReO_6, Phys. Rev. B **81**, 064436 (2010).

[58] G. Kresse and D. Joubert, From ultrasoft pseudopotentials to the projector augmented-wave method, Phys. Rev. B **59**, 1758 (1999).

[59] G. Kresse and J. Hafner, *Ab initio* molecular dynamics for liquid metals, Phys. Rev. B **47**, 558 (1993).

[60] J. P. Perdew, K. Burke, and M. Ernzerhof, Generalized gradient approximation made simple, Phys. Rev. Lett. **77**, 3865 (1996).

[61] J. P. Perdew, A. Ruzsinszky, G. I. Csonka, O. A. Vydrov, G. E. Scuseria, L. A. Constantin, X. Zhou, and K. Burke, Restoring the density-gradient expansion for exchange in solids and surfaces, Phys. Rev. Lett. **100**, 136406 (2008).

[62] O. K. Andersen, Linear methods in band theory, Phys. Rev. B **12**, 3060 (1975).

[63] N. Marzari, A. A. Mostofi, J. R. Yates, I. Souza, and D. Vanderbilt, Maximally localized Wannier functions: Theory and applications, Rev. Mod. Phys. **84**, 1419 (2012).